Conformational stabilities of dicyclopropyl methane determined from variable temperature infrared spectra of rare gas solutions and ab initio calculations

ARTICLE *in* JOURNAL OF MOLECULAR STRUCTURE · JANUARY 2001

Impact Factor: 1.6 · DOI: 10.1016/S0022-2860(00)00711-0

5 AUTHORS, INCLUDING:

Todor K Gounev
University of Missouri - Kansas City
77 PUBLICATIONS **576** CITATIONS
SEE PROFILE

Charles J Wurrey
University of Missouri - Kansas City
78 PUBLICATIONS **997** CITATIONS
SEE PROFILE

ELSEVIER

Journal of Molecular Structure 559 (2001) 273–293

Journal of
MOLECULAR
STRUCTURE

www.elsevier.nl/locate/molstruc

Conformational stabilities of dicyclopropyl methane determined from variable temperature infrared spectra of rare gas solutions and ab initio calculations

T.K. Gounev, Y.E. Nashed, A. Koomer, C.J. Wurrey, J.R. Durig*

Department of Chemistry, University of Missouri–Kansas City, 5100 Rockhill Road, Kansas City, MO 64110-2499, USA

Received 28 June 2000; accepted 27 July 2000

Abstract

The infrared (3500–40 cm^{-1}) spectra of gaseous and solid dicyclopropyl methane, (c-$C_3H_5)_2CH_2$, along with the Raman (3500–30 cm^{-1}) spectra of the liquid and solid phases of this molecule have been recorded. Three of the four possible conformers have been identified in the fluid phases, and they are the *gauche–gauche* rotamer with C_2 symmetry, *gauche–gauche* rotamer with C_s symmetry, and the *gauche–cis* rotamer with C_1 symmetry. Variable temperature (−55 to −145°C) studies of the infrared spectra of the sample dissolved in liquid xenon and krypton have been carried out. Utilizing six different combinations of pairs of bands from the C_2 and C_s conformers, the average value of ΔH, the enthalpy difference between these two conformers, is 239 ± 13 cm^{-1} (2.86 ± 0.16 kJ/mol) from the xenon solution and 211 ± 12 cm^{-1} (2.52 ± 0.14 kJ/mol) from the krypton solution, with the C_2 form the more stable rotamer in both solvents. The enthalpy difference for the *gauche–cis* form was obtained from the temperature dependence of the relative intensities of three of the fundamentals of this conformer with three fundamentals of the C_2 form and two fundamentals of the C_s form, from which a value of 479 ± 84 cm^{-1} (5.73 ± 1.00 kJ/mol) was obtained between the C_2 rotamer and this less stable C_1 form. A complete vibrational assignment is proposed for the C_2 conformer and most of the fundamentals have been assigned for the C_s conformer, utilizing predictions of fundamental frequencies, infrared intensities, and Raman activities from MP2/6-31G(d) ab initio calculations. The structural parameters, dipole moments and conformational stabilities of the four possible conformers of dicyclopropyl methane have been obtained from RHF/6-31G(d), MP2/6-31G(d) and MP2/6-311+G(d,p) ab initio calculations, with the latter two incorporating full electron correlation. The predicted conformational stabilities are consistent with the experimental results. These experimental and theoretical results are compared to the corresponding quantities of some similar molecules.

Keywords: Conformational stability; ab initio calculations; FT-IR spectra; dicyclopropyl methane

1. Introduction

The monosubstituted methyl cyclopropanes, c-$C_3H_5CH_2X$, where X = F, Cl, Br, CH_3, CN, and C≡C–H provide an interesting series of molecules which have *cis* (X over the three-membered ring) and *gauche* conformers present in the fluid phases. When X is a halogen atom or methyl group the predominant conformer at ambient temperature is the *gauche* form with relatively small percentages of the *cis* rotamer (10, 12, 8 and 2% for X = F [1], Cl [2], Br [2] and CH_3 [3], respectively). However, for X = CN,

* Corresponding author. Tel.: +1-816-235-6038; fax: +1-816-235-5502.

E-mail address: durigj@umkc.edu (J.R. Durig).

0022-2860/01/$ - see front matter
PII: S0022-2860(00)00711-0

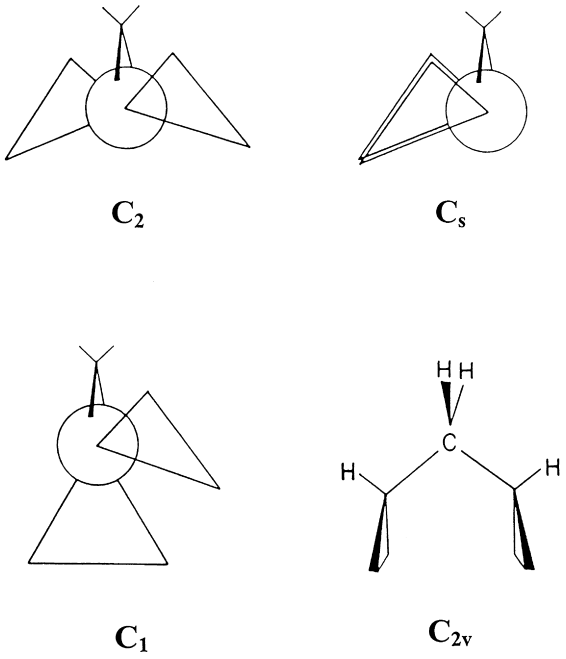

Fig. 1. Four possible conformations of dicyclopropyl methane.

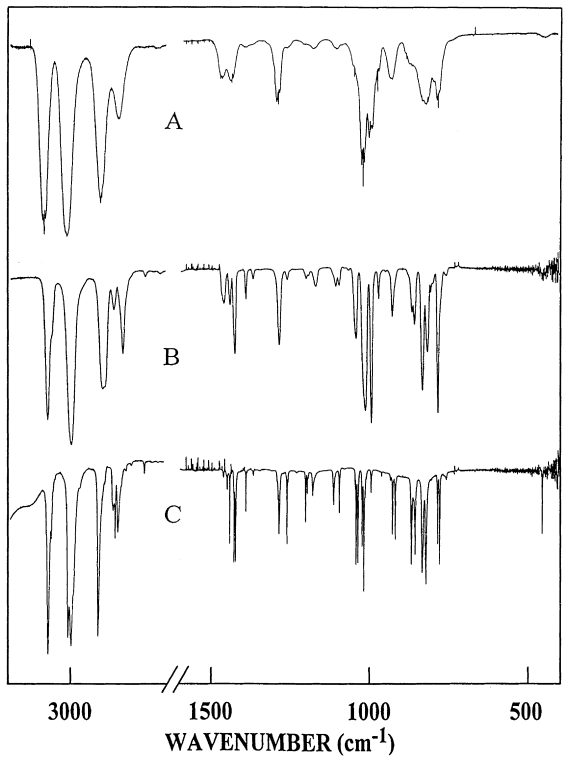

Fig. 2. Infrared spectra of dicyclopropyl methane in the: (A) gas; (B) amorphous solid; and (C) annealed solid.

cyanomethylcyclopropane [4], and C≡C–H, ethynylmethylcyclopropane [5], the amount of the *cis* conformer present at ambient temperature increases to 40 and 48%, respectively. In the initial conformational investigation of ethynylmethylcyclopropane from a microwave study [6], it was suggested that the electronegativity of the substituent X was the major factor determining the percent of the *cis* conformer present in these monosubstituted methylcyclopropane molecules. However, recent studies [1] of fluoromethylcyclopropane indicated that electronegativity is probably not the controlling factor. It is very possible that an interaction of the X group with the three-membered ring is the most important factor determining the amount of *cis* rotamer present. Therefore, we have investigated the conformational stability of dicyclopropyl methane, $(c\text{-}C_3H_5)_2CH_2$, where each of the cyclopropane rings may in turn be considered as the X group. Earlier conformational studies of this molecule [7] were carried out without ab initio predictions to indicate where the fundamentals could be expected for the four possible conformers of dicyclopropyl methane (Fig. 1). Therefore, we have carried out infrared and Raman investigations of the fluid and solid states. Of particular importance were the temperature dependent infrared spectral studies of rare gas solutions.

Ab initio calculations have been carried out utilizing the 6-31G(d) basis set at the restricted Hartree–Fock level and with full electron correlation by the perturbation method [8] to second order (MP2) to obtain optimized geometries, conformational stabilities, harmonic force fields, infrared intensities, Raman activities and depolarization ratios. The results of these spectroscopic and theoretical studies are reported herein.

2. Experimental

The sample of dicyclopropyl methane was obtained from Chemical Samples Co. at a stated purity of 99%. The sample was further purified on a low-temperature, low-pressure fractionation column. The purity was

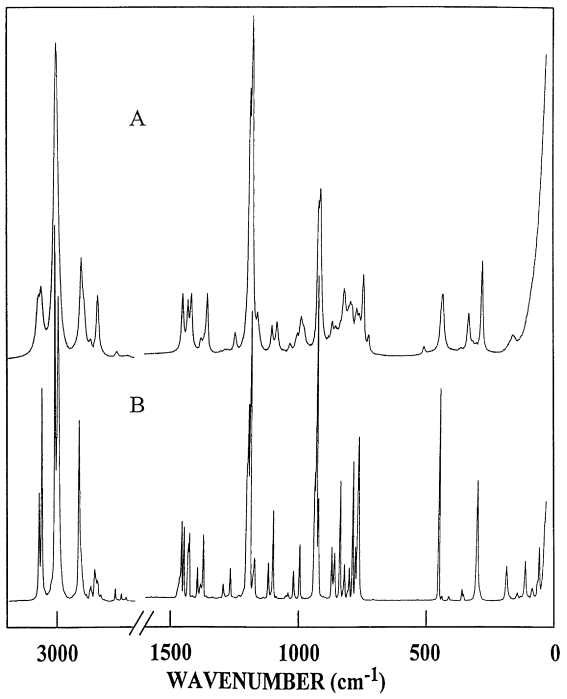

Fig. 3. Raman spectra of dicyclopropyl methane in the: (A) liquid; and (B) annealed solid.

verified by a comparison of the infrared spectrum to that previously reported [7].

The mid-infrared spectra of the gas and solid (Fig. 2) were obtained from 3200 to 300 cm^{-1} using a Perkin–Elmer model 2000 Fourier transform spectrometer equipped with a Ge/CsI beamsplitter and a DTGS detector. The gas was contained in a 10 cm cell fitted with CsI windows. The spectrum was obtained at a resolution of 0.5 cm^{-1} from 64 co-added scans of the sample and reference, and the interferograms were transformed with a boxcar truncation function. The spectrum of the solid was obtained by condensing the sample onto a boiling liquid nitrogen cooled CsI plate contained in an evacuated cell equipped with CsI windows, and 256 scans were collected for both the reference and sample interferograms at 1 cm^{-1} resolution and then transformed with a boxcar truncation function.

The mid-infrared spectra of the sample dissolved in liquified xenon and krypton as a function of temperature were recorded on a Bruker model IFS 66 Fourier transform spectrometer equipped with a Globar source, a Ge/KBr beamsplitter and a DTGS detector. In all cases, 100 interferograms were collected at 1.0 cm^{-1} resolution, averaged and transformed with a boxcar truncation function. For these studies, a specially designed cryostat cell was used. It consisted of a copper cell with a path length of 4 cm with wedged silicon windows sealed to the cell with indium gaskets. The copper cell was enclosed in an evacuated chamber fitted with KBr windows. The temperature was maintained with boiling liquid nitrogen and monitored with two Pt thermoresistors. The complete cell was connected to a pressure manifold, allowing the filling and evacuation of the system. After cooling to the desired temperature, a small amount of the compound was condensed into the cell. Next, the system was pressurized with the noble gas, which immediately started to condense in the cell, allowing the compound to dissolve.

The Raman spectra (Fig. 3) were recorded on a SPEX model 1403 spectrophotometer equipped with a Spectra-Physics model 164 argon ion laser operating on the 514.5 nm line. The laser power used was 0.5 W with a spectral bandpass of 3 cm^{-1}. The spectrum of the liquid was recorded with the sample sealed in a Pyrex glass capillary held in a Miller–Harney apparatus [9]. Depolarization measurements were obtained for the liquid sample using a standard Ednalite 35 mm camera polarizer with 38 mm of free aperture affixed to the SPEX instrument. Depolarization ratio measurements were checked by measuring the state of polarization of the Raman bands of CCl_4 immediately before depolarization measurements were made on the liquid sample. The measurements of the Raman frequencies are expected to be accurate to ± 2 cm^{-1}. All of the observed bands in both the infrared and Raman spectra, along with the proposed assignments, are listed in Table 1.

3. Ab initio calculations

The LCAO-MO-SCF restricted Hartree–Fock calculations were performed with the GAUSSIAN-98 program [10] using Gaussian-type basis functions. The energy minima with respect to nuclear coordinates were obtained by the simultaneous relaxation of all of the geometric parameters consistent with the symmetry restrictions using the gradient method of Pulay [11].

Table 1
Observed[a] infrared and Raman wavenumbers (cm^{-1}) for dicyclopropyl methane

Infrared						Raman				Assignment	
Gas	Rel. int.	Xenon soln.	Rel. int.	Annealed solid	Rel. int.	Liquid	Rel. int. and depol.	Solid	Rel. int.	ν_i[b]	Approximate description
3091 R				3070	s	3076	m,p	3073	m	ν_1, ν_{27}	CH_2 antisymmetric stretch
3086 Q,A	vs	3077	vs								
3081 P				3061	w	3066	m,dp	3063	s	ν_2,ν_{28}	CH_2 antisymmetric stretch
				3006	s	3006	vs,p	3010	vs	ν_3,ν_{29}	CH stretch
3014		3004	vs								
				2997	s			2998	vs	ν_4,ν_{30}	CH_2 symmetric stretch
				2990	m					ν_5,ν_{31}	CH_2 symmetric stretch
2909 R											
2905 Q	s	2906	s	2913	s	2908	m,p	2915	m	ν_{32}	*CH_2 antisymmetric stretch
2900 P											
		2896	s	2893	w	2897	m,p	2906	vw	ν_6	*CH_2 symmetric stretch
1470 Q	w	1464	w							ν'_9	
		1461	w	1460	w	1464	w,p	1453	w	ν_7	CH_2 deformation
1464 Q	w	1460	w							ν_{33}, ν'_{33}	CH_2 deformation
1445 Q	w	1441	w	1440	w	1442	w,p	1443	w	ν_8, ν'_8	*CH_2 deformation
1440 R											
1434 Q	w			1426	m			1427	w	ν_{34}, ν'_7, ν'_{34}	CH_2 deformation
1430 P		1428	m			1429	w,dp				
				1421	m			1423	w	ν_9	CH_2 deformation
1396 R											
1392 min, B	vw	1390	w	1389	w	1392	vw,p	1391	vw	ν_{35}, ν'_{35}	CH in-plane bend
1388 P											
1372	vw	1367	vw	1366	vw	1366	w,p	1368	w	ν_{10}, ν'_{10}	CH in-plane bend
		1312	vw			1315	vw,p			ν''_{36}	
1301 R											
1297 Q	w	1295	w							ν'_{36}	
1292 R											
1287 Q, A	w	1285	m	1283	w			1291	vw	ν_{36}	*CH_2 wag
1283 P											
		1257	vw	1258	w	1258	vw,p	1263	vw	ν_{11}	*CH_2 twist
1258 R											
1253 Q	vw	1250	vw							ν'_{11}	
1247 P											
1206 Q	vw	1204	vw	1200	w	1205	s,p	1201	m	ν_{37}, ν'_{12}	Ring breathing
								1197	m		
		1199	vw	1195	vw	1197	s,p	1189	s	ν_{12}	Ring breathing
1199 Q	vw	1195	vw							ν'_{37}	
		1192	vw							ν'_{13}	

Table 1 (*continued*)

Infrared						Raman				Assignment	
Gas	Rel. int.	Xenon soln.	Rel. int.	Annealed solid	Rel. int.	Liquid	Rel. int. and depol.	Solid	Rel. int.	ν_i[b]	Approximate description
1177 Q	vw	1174	vw	1178						ν_{38}	CH_2 twist
1173 Q	vw	1169	w	1174	vw	1170	w,p	1170	w	ν_{13}, ν'_{15}	CH_2 twist
1169 Q	vw	1167	vw	1165	vw			1169	w	ν_{39}, ν'_{38}	CH_2 twist
1107 Q	vw	1103	w	1112	w	1114	vw,p	1116	w	ν_{14}, ν'_{14}	CH out-of-plane bend
1103 Q	vw									ν_{40}, ν'_{40}	CH out-of-plane bend
		1093	w	1093	w	1094	w,p			ν_{15}	CH_2 twist
		1064	vw							ν'_{43}	
1049 R		1045								ν'_{17}	
1046 Q	w	1042	s	1043	vw	1043	vw,p	1043	vw	ν_{41}	CH_2 wag
1043 Q	w	1039	w	1034	m			1038	vw	ν_{16}, ν'_{16}	CH_2 wag
1024 Q	s	1020	s	1021	w			1018	vw	ν_{17}, ν'_{41}	CH_2 wag
1019 Q,A/C	s	1015	s	1015	m	1016	w,dp			ν_{42}	CH_2 wag
1015 P											
1014 Q	s	1010	s			1002	w,p			ν'_{42}	
999 R											
994 Q, A	m	994	s	993	vw	988	w,dp	993	w	ν_{43}	CC antisymmetric stretch
990 P											
979 R											
973 Q, A	w	970	m							ν'_{39}	
969 P											
		958	vw							ν''_{18}	
933 Q	w	929	m	934	w	935	m,p	937	m	ν_{18}, ν'_{18}	Ring deformation
930 ctr				927	m	928	m,p	930	vs	ν_{19}	Ring deformation
927		923	w	918	m	921	sh,m,dp	922	m	ν_{44}	Ring deformation
887 R											
883 Q, A	vw	879	vw			878	w,dp			ν'_{44}	
876 R											
867 Q	w	865	m	868	m	864	w,dp	868	w	ν_{45}	*CH_2 rock
		851	w	856	m	848	w	857	w		
849		846	w								
		833	s	834	m	832	w,p	836	m	ν_{20}	CH_2 rock
838 Q	w	831	m							ν'_{19}	
833 P											
822 R											
816 Q	w	815	m							ν'_{47}	
811 Q	w			822	m	813	w,dp	818	vw	ν_{46}	CH_2 rock
808 Q	w	808	w			808	w,dp			ν'_{46}	
797		793	vw			804	w,p	799	vw	ν_{21}	CH_2 rock
788 R											

Table 1 (*continued*)

Infrared						Raman				Assignment	
Gas	Rel. int.	Xenon soln.	Rel. int.	Annealed solid	Rel. int.	Liquid	Rel. int. and depol.	Solid	Rel. int.	ν_i [b]	Approximate description
784 Q,A/C	m	784	vs	785	w	783	w,dp	787	m	ν_{47}	Ring deformation
780 Q	w	780	w							ν'_{21}	
		773	w	779	m	773	w,dp	776	w	ν_{48}, ν'_{48}	CH_2 rock
		754	vw	757	vw	757	m,p			ν_{22}, ν'_{22}	CC symmetric stretch
		736	vw			738	vw,p			ν''_{22}	
		518	vw			521	vw,p			ν''_{49}	
447		452	vw	453	w	450	w,p	450	s	ν_{23}, ν'_{23}	Ring-C out-of-plane bend
				410	vw			409	vw	ν_{49}	Ring-C in-plane bend
				348	w	345	w,p	350	vw	ν'_{24}, ν_{50}	Ring-C out-of-plane bend
				291	vw	293	m,p	294	m	ν_{24}	Ring-C in-plane bend
				231	vw						
				184	vw	172	vw,p	182	vw	ν_{25}, ν'_{25}	CCC bend
								140		ν_{51}	Torsion
								108		ν_{26}	Torsion
								80			Lattice modes
				67				61			
								53			

[a] Abbreviations used: s, strong; m, moderate; w, weak; v, very; bd, broad; sh, shoulder; p, polarized; dp, depolarized; A, B, and C refer to infrared band envelopes; P,Q, and R refer to the rotational-vibrational branches.

[b] ν_i, ν'_i and ν''_i refer to the C_2, C_s and C_1 conformers, respectively, and the asterisk on the CH_2 group indicates the group not in the ring.

Table 2
Structural parameters (bond distances in Å, bond angles in degrees), rotational constants (MHz), dipole moments (debye) and energy (Hartree) for dicyclopropyl methane

	RHF/6-31G(d)				MP2/6-31G(d)				MP2/6-311+G(d,p)			
	C_2	C_s	C_1	C_{2v}	C_2	C_s	C_1	C_{2v}	C_2	C_s	C_1	C_{2v}
C_1C_2	1.515	1.515	1.521	1.525	1.508	1.509	1.515	1.519	1.509	1.510	1.518	1.520
C_1C_3	1.515	1.515	1.515	1.525	1.508	1.509	1.509	1.519	1.509	1.510	1.510	1.520
C_2C_4	1.497	1.497	1.498	1.497	1.502	1.502	1.503	1.502	1.507	1.508	1.508	1.508
C_3C_5	1.497	1.497	1.498	1.497	1.502	1.502	1.503	1.502	1.507	1.508	1.509	1.508
C_2C_6	1.499	1.497	1.497	1.500	1.503	1.502	1.502	1.505	1.508	1.507	1.508	1.511
C_3C_7	1.499	1.497	1.499	1.500	1.503	1.502	1.504	1.505	1.508	1.507	1.509	1.511
C_4C_6	1.500	1.500	1.500	1.501	1.505	1.505	1.505	1.506	1.513	1.513	1.513	1.514
C_5C_7	1.500	1.500	1.498	1.501	1.505	1.505	1.502	1.506	1.513	1.513	1.510	1.514
CH_8	1.088	1.088	1.088	1.088	1.099	1.099	1.099	1.099	1.099	1.099	1.099	1.098
CH_9	1.088	1.088	1.088	1.088	1.099	1.099	1.099	1.099	1.099	1.098	1.099	1.098
CH_{10}	1.078	1.078	1.078	1.078	1.088	1.089	1.088	1.089	1.088	1.087	1.088	1.088
CH_{11}	1.078	1.078	1.077	1.078	1.088	1.089	1.088	1.089	1.088	1.087	1.086	1.088
CH_{12}	1.076	1.076	1.076	1.076	1.085	1.085	1.085	1.085	1.084	1.084	1.084	1.084
CH_{13}	1.076	1.076	1.076	1.076	1.085	1.085	1.085	1.085	1.084	1.084	1.084	1.084
CH_{14}	1.077	1.077	1.076	1.075	1.086	1.086	1.084	1.084	1.085	1.085	1.084	1.083
CH_{15}	1.077	1.077	1.077	1.075	1.086	1.086	1.086	1.084	1.085	1.085	1.085	1.083
CH_{16}	1.076	1.076	1.076	1.076	1.085	1.085	1.085	1.085	1.084	1.084	1.084	1.084
CH_{17}	1.076	1.076	1.076	1.076	1.085	1.085	1.085	1.085	1.084	1.084	1.084	1.084
CH_{18}	1.077	1.076	1.075	1.073	1.086	1.085	1.083	1.081	1.085	1.084	1.083	1.081
CH_{19}	1.077	1.076	1.076	1.073	1.086	1.085	1.086	1.081	1.085	1.084	1.085	1.081
$C_3C_1C_2$	112.8	113.2	116.7	123.5	112.0	112.7	115.6	122.5	112.1	112.7	115.4	122.3
$C_1C_2C_4$	120.6	120.6	123.4	124.8	120.4	120.3	122.3	123.9	119.9	119.9	121.9	123.7
$C_1C_3C_5$	120.6	120.6	119.5	124.8	120.4	120.3	119.2	123.9	119.9	119.9	118.8	123.7
$C_1C_2C_6$	120.5	121.2	123.7	128.2	119.6	120.2	122.4	127.7	118.9	119.8	122.2	127.5
$C_1C_3C_7$	120.5	121.2	121.0	128.2	119.6	120.2	120.3	127.7	118.9	119.8	119.7	127.5
$C_2C_1H_8$	109.3	109.4	108.1	106.2	109.3	109.0	108.8	106.4	108.9	108.9	108.7	106.5
$C_2C_1H_9$	109.4	109.1	108.3	107.0	109.9	109.8	108.7	107.4	109.9	109.7	108.8	107.4
$C_3C_1H_8$	109.4	109.4	108.6	107.0	109.9	109.0	108.9	17.4	109.9	108.9	109.4	107.4
$C_3C_1H_9$	109.3	109.1	108.5	106.2	109.3	109.8	108.1	106.4	108.9	109.7	107.9	106.5
$H_8C_1H_9$	106.3	106.3	106.1	105.5	106.3	106.3	106.2	105.5	106.7	106.7	106.5	105.8
$C_1C_2H_{10}$	114.0	113.9	111.9	109.7	114.4	114.4	113.0	110.5	115.0	114.9	113.5	110.9
$C_1C_3H_{11}$	114.0	113.9	114.8	109.7	114.4	114.4	115.3	110.5	115.0	114.9	115.9	110.9
$C_4C_2H_{10}$	115.7	115.4	114.2	113.0	116.1	115.6	114.4	113.1	116.0	115.6	114.4	113.7
$C_5C_3H_{11}$	115.7	115.4	114.9	113.0	116.1	115.6	114.9	113.1	116.0	115.6	114.9	113.1
$C_6C_2H_{10}$	115.6	115.4	114.5	112.9	115.7	115.6	114.8	112.9	115.8	115.6	114.7	112.8
$C_7C_3H_{11}$	115.6	115.4	115.6	112.9	115.7	115.6	115.8	112.9	115.8	115.6	115.7	112.8
$C_2C_4H_{12}$	118.5	118.6	118.1	118.1	118.6	118.7	118.2	118.3	118.4	118.5	117.9	118.0
$C_3C_5H_{13}$	118.5	118.6	118.4	118.1	118.6	118.7	118.5	118.3	118.4	118.5	118.2	118.0
$C_2C_4H_{14}$	118.0	117.9	118.9	118.4	117.5	117.5	118.4	117.8	117.2	117.1	118.1	117.6

Table 2 (*continued*)

	RHF/6-31G(d)				MP2/6-31G(d)				MP2/6-311+G(d,p)			
	C_2	C_s	C_1	C_{2v}	C_2	C_s	C_1	C_{2v}	C_2	C_s	C_1	C_{2v}
$C_3C_5H_{15}$	118.0	117.9	117.9	118.4	117.5	117.5	117.5	117.8	117.2	117.1	117.1	117.6
$C_2C_6H_{16}$	118.6	118.6	118.2	117.4	118.7	118.7	118.3	117.4	118.5	118.5	117.9	117.2
$C_3C_7H_{17}$	118.6	118.6	118.6	117.4	118.7	118.7	118.7	117.4	118.5	118.5	118.5	117.2
$C_2C_6H_{18}$	118.0	118.1	118.4	120.0	117.7	117.6	117.7	119.8	117.1	117.2	117.6	119.6
$C_3C_9H_{19}$	118.0	118.1	117.8	120.0	117.5	117.6	117.3	119.8	117.1	117.2	116.8	119.6
$C_6C_4H_{12}$	118.3	118.3	118.4	118.4	118.3	118.4	118.5	118.3	117.9	117.9	118.4	118.0
$C_7C_5H_{13}$	118.3	118.3	118.3	118.4	118.3	118.4	118.3	118.3	117.9	117.9	117.9	118.0
$C_6C_4H_{14}$	117.8	117.8	117.7	118.0	117.7	117.7	117.5	117.9	117.4	117.4	117.1	117.6
$C_7C_5H_{15}$	117.8	117.8	117.9	118.0	117.7	117.7	117.8	117.9	117.4	117.4	117.5	117.6
$C_4C_6H_{16}$	118.3	118.3	118.3	118.1	118.3	118.3	118.4	118.1	117.9	117.9	117.9	117.6
$C_5C_7H_{17}$	118.3	118.3	118.3	118.1	118.3	118.3	118.3	118.0	117.9	117.9	117.9	117.6
$C_4C_6H_{18}$	117.8	117.8	117.5	118.1	117.7	117.8	117.2	118.2	117.3	117.4	116.9	117.8
$C_5C_7H_{19}$	117.8	117.8	117.8	118.1	117.7	117.8	117.7	118.2	117.3	117.4	117.4	117.8
$H_{12}CH_{14}$	113.9	113.9	113.7	113.7	114.2	114.2	114.0	114.1	115.0	115.0	114.8	114.9
$H_{13}CH_{15}$	113.9	113.9	113.9	113.7	114.2	114.2	114.2	114.1	115.0	115.0	115.1	114.9
$H_{16}CH_{18}$	113.9	113.9	114.1	113.3	114.2	114.1	114.6	113.6	115.0	114.9	115.3	114.3
$H_{17}CH_{19}$	113.9	113.9	113.9	113.3	114.2	114.1	114.3	113.6	115.0	114.9	115.1	114.3
τ_1	120.7	123.3	2.0	18.1	118.4	120.6	2.4	18.4	118.3	120.9	2.95	18.5
τ_2	120.7	123.3	124.1	181	118.4	120.6	122.0	18.4	118.3	120.9	122.1	18.5
A	7836	7021	5990	4714	7728	6870	5891	4655	7695	6840	5867	4634
B	1283	1417	1591	1885	1304	1453	1640	1942	1302	1450	1640	1936
C	1261	1298	1470	1688	1280	1326	1508	1740	1279	1324	1509	1733
$\lvert\mu_a\rvert$	0.000	0.000	0.070	0.000	0.000	0.000	0.078	0.000	0.000	0.000	0.053	0.000
$\lvert\mu_b\rvert$	0.056	0.063	0.104	0.258	0.069	0.059	0.096	0.251	0.058	0.085	0.135	0.315
$\lvert\mu_c\rvert$	0.000	0.158	0.014	0.000	0.000	0.177	0.008	0.000	0.000	0.197	0.017	0.000
$\lvert\mu_t\rvert$	0.056	0.170	0.126	0.258	0.069	0.186	0.124	0.251	0.058	0.214	0.146	0.315
$-(E+271)$	0.99821	0.99717	0.99468	0.98378	1.94163	1.94067	1.93971	1.92936	2.32939	2.23198	2.23099	2.22086
ΔE (cm^{-1})	0	228	773	3165	0	211	421	2692	0	210	427	2652

The structural optimizations were carried out with initial parameters taken from those of fluoromethylcyclopropane [1]. The 6-31G(d) and 6-311+G(d,p) basis sets were employed at the level of restricted Hartree–Fock (RHF) and/or Møller–Plesset (MP2) to second order with full electron correlation [8]. The determined structural parameters are listed in Table 2.

In order to obtain a more complete description of the molecular motions involved in the normal modes of dicyclopropyl methane, a normal coordinate analysis has been carried out. The force fields in Cartesian coordinates were calculated by the GAUSSIAN-98 program [10] with the MP2/6-31G(d) basis set. Internal coordinates (Fig. 4) were used to calculate the *G* and *B* matrices using the structural parameters given in Table 2. Using the *B* matrix [12], the force field in Cartesian coordinates was then converted to a force field in internal coordinates, and the pure ab initio vibrational frequencies were reproduced [13]. The force constants for all four conformers can be obtained from the authors. Subsequently, scaling factors of 0.9 for stretches and bends and 1.0 for the torsional coordinates, and the geometric average of scaling factors for interaction force constants, were used to obtain the fixed scaled force field and resultant wavenumbers. A set of symmetry coordinates was used (Table 3) to determine the corresponding potential energy distributions (PEDs). A comparison between the observed and calculated frequencies of dicyclopropyl methane along with the calculated infrared intensities, Raman activities, depolarization ratios and PEDs are given in Table 4.

Raman and infrared spectra for dicyclopropyl methane were simulated using the calculated frequencies, scattering activities and intensities determined from the ab initio calculations. The GAUSSIAN-98 program [10] with the option of calculating the polarizability derivatives (RHF/6-31G(d)) was used. The Raman scattering cross-sections, $\partial\sigma_j/\partial\Omega$, which are proportional to the Raman intensities, can be calculated from the scattering activities and the predicted frequencies for each normal mode using the relationship [14,15]

$$\frac{\partial\sigma_j}{\partial\Omega} = \left(\frac{2^4\pi^4}{45}\right)\left(\frac{(\nu_0 - \nu_j)^4}{1 - \exp\left[\frac{-\mathrm{h}c\nu_j}{\mathrm{k}T}\right]}\right)\left(\frac{\mathrm{h}}{8\pi^2 c\nu_j}\right)S_j$$

where ν_0 is the exciting frequency, ν_j is the vibrational frequency of the *j*th normal mode, h, *c* and k are universal constants, and S_j is the corresponding Raman scattering activity. The evaluation of Raman activities by using the analytical gradient methods has been developed previously [16,17].

$$S_j = g_j(45\alpha_j^2 + 7\beta_j^2)$$

where g_j is the degeneracy of the vibrational mode *j*, α_j is the derivative of the isotropic polarizability, and β_j is that of the anisotropic polarizability. To obtain the polarized Raman scattering cross-section, the polarizabilities are incorporated into S_j by $S_j[(1-\rho_j)/(1+\rho_j)]$ where ρ_j is the depolarization ratio of the *j*th normal mode. The Raman scattering cross-sections and calculated fixed scaled frequencies are used together with a Lorentzian line shape function to obtain the simulated spectrum. The predicted Raman spectra of the pure *gauche–gauche* (C_2), *gauche–gauche* (C_s) and *gauche–cis* (C_1) conformers are shown in Fig. 5C–E, respectively. The predicted Raman spectrum of the mixture of the three conformers with ΔH values of 225 and 479 cm^{-1} for the C_1/C_2 and C_1/C_s conformer pairs, respectively, is shown in Fig. 5B which should be compared to the experimental spectrum of the liquid (Fig. 5A). The utilized ΔH values are taken from the temperature dependent studies of the spectra of the krypton and xenon solutions.

Infrared intensities were also calculated based on the dipole moment derivatives with respect to the Cartesian coordinates. The derivatives were taken from the ab initio calculations at the MP2/6-31G(d) level and transformed to normal coordinates by

$$\left(\frac{\partial\mu_\mu}{\partial Q_i}\right) = \sum_j \left(\frac{\partial\mu_\mu}{\partial X_j}\right)L_{ji}$$

where Q_i is the *i*th normal coordinate, X_j is the *j*th Cartesian displacement coordinate, and L_{ji} is the transformation matrix between the Cartesian displacement coordinates and normal coordinates. The infrared intensities were then calculated by

$$I_i = \frac{N\pi}{3c^2}\left[\left(\frac{\partial\mu_x}{\partial Q_i}\right)^2 + \left(\frac{\partial\mu_y}{\partial Q_i}\right)^2 + \left(\frac{\partial\mu_z}{\partial Q_i}\right)^2\right]$$

In Fig. 6C–E, the predicted infrared spectra of the *gauche–gauche* (C_2), *gauche–gauche* (C_s) and

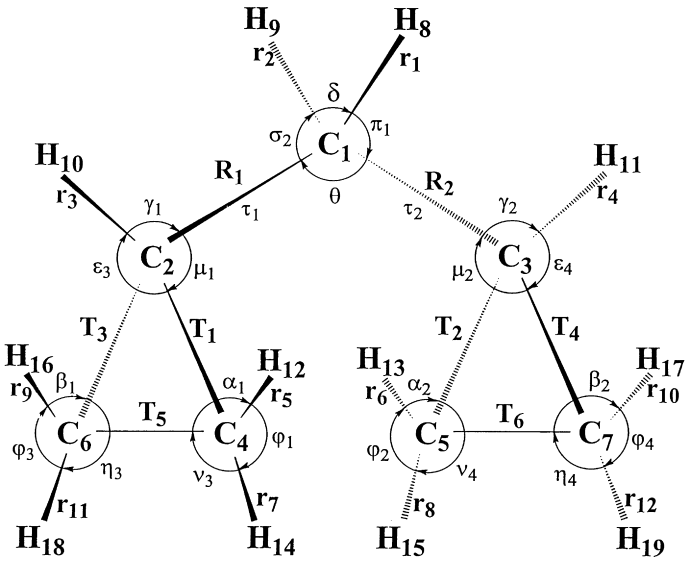

Fig. 4. Internal coordinates of dicyclopropyl methane.

gauche–cis (C_1) conformers, respectively, are shown. The combination of the spectra of the three identified conformers present at ambient temperature with ΔH values of 211 cm^{-1} between the C_2 and C_s conformers and 479 cm^{-1} between the C_2 and C_1 conformers is shown in Fig. 6B, and the experimental spectrum of the sample dissolved in liquid xenon is shown in Fig. 6A for comparison. A major difference is noted in the 900–1100 cm^{-1} spectral region, which will be discussed more fully in the following section.

4. Conformational stability

The ab initio energy calculations at the MP2 level showed that the *cis–cis* (C_{2v}) conformer has energy in excess of 2500 cm^{-1} higher than that of the most stable C_2 form. The C_s and C_1 conformers are predicted approximately 200 and 400 cm^{-1}, respectively, higher in energy than the C_2 rotamer. Therefore, the expectation is to observe only spectral bands due to the C_2 and C_s forms, and possibly very weak features due to the C_1 conformation.

The Raman spectra provide strong evidence for the existence of the C_1 conformer. From Fig. 3 it is clear that the weak bands at 521 and 738 cm^{-1} in the spectrum of the liquid are not present in the spectrum of the annealed solid. Only the C_1 conformer is expected to produce a band in the 500 cm^{-1} region due to the ring-C in-plane bending mode, which should be relatively strong in the Raman spectrum (Table 5). Another very strong Raman fundamental of the C_1 rotamer, the CC symmetric stretch, is attributed to the band at 738 cm^{-1}. The corresponding fundamentals of the C_2 and C_s conformers are expected to be overlapped ~20 cm^{-1} higher in frequency and are observed as a much stronger band at 757 cm^{-1}. No other bands are expected in the 750–700 cm^{-1} range.

The vast amount of the remaining fundamentals belongs to the C_2 and C_s conformers. In the low 900 cm^{-1} region there are three ring deformation modes of the C_2 and one of the C_s conformers (Table 4) expected to be quite strong in the Raman spectra. Three clearly distinguishable bands at 937, 930 and 922 cm^{-1} are observed in the Raman spectrum of the annealed solid, suggesting that the C_2 conformer is the most stable structure in the solid phase. In addition, a fundamental of the C_s conformer is expected to appear at ~973 cm^{-1} with relatively high infrared intensity. The observed band is at 970 cm^{-1} in the spectrum of the xenon solution and it clearly disappears upon annealing. Therefore, the conclusion is that the C_2, C_s and C_1 conformers are present in the fluid phases and only the C_2 form is

Table 3
Symmetry coordinates (not normalized; asterisk on the CH_2 group indicates the one not in the rings; see Fig. 4 for internal coordinate definitions) for dicyclopropylmethane (C_2 conformer)

Species	Description	Symmetry coordinate[a]
A	CH_2 antisymmetric stretch	$S_1 = r_5 + r_6 - r_7 - r_8$
	CH_2 antisymmetric stretch	$S_2 = r_{10} + r_9 - r_{11} - r_{12}$
	CH stretch	$S_3 = r_3 + r_4$
	CH_2 symmetric stretch	$S_4 = r_5 + r_6 + r_7 + r_8$
	CH_2 symmetric stretch	$S_5 = r_9 + r_{10} + r_{11} + r_{12}$
	$^*CH_2$ symmetric stretch	$S_6 = r_1 + r_2$
	CH_2 deformation	$S_7 = 4\varphi_1 + 4\varphi_2 - \alpha_1 - \alpha_2 - \alpha_3 - \alpha_4 - \nu_1 - \nu_2 - \nu_3 - \nu_4$
	$^*CH_2$ deformation	$S_8 = 4\delta - \pi_1 - \pi_2 - \sigma_1 - \sigma_2$
	CH_2 deformation	$S_9 = 4\varphi_3 + 4\varphi_4 - \beta_1 - \beta_2 - \beta_3 - \beta_4 - \eta_1 - \eta_2 - \eta_3 - \eta_4$
	CH in-plane bend	$S_{10} = 2\gamma_1 + 2\gamma_2 - \epsilon_1 - \epsilon_2 - \epsilon_3 - \epsilon_4$
	$^*CH_2$ twist	$S_{11} = \sigma_1 - \sigma_2 - \pi_1 + \pi_2$
	Ring breathing	$S_{12} = T_1 + T_2 + T_3 + T_4 + T_5 + T_6$
	CH_2 twist	$S_{13} = \beta_1 + \beta_2 - \beta_3 - \beta_4 - \eta_1 - \eta_2 + \eta_3 + \eta_4$
	CH out-of-plane bend	$S_{14} = \epsilon_1 + \epsilon_2 - \epsilon_3 - \epsilon_4$
	CH_2 twist	$S_{15} = \alpha_1 + \alpha_2 - \alpha_3 - \alpha_4 - \nu_1 - \nu_2 + \nu_3 + \nu_4$
	CH_2 wag	$S_{16} = \alpha_1 + \alpha_2 - \alpha_3 - \alpha_4 + \nu_1 + \nu_2 - \nu_3 - \nu_4$
	CH_2 wag	$S_{17} = \beta_1 + \beta_2 - \beta_3 - \beta_4 + \eta_1 + \eta_2 - \eta_3 - \eta_4$
	Ring deformation	$S_{18} = 2T_5 + 2T_6 - T_1 - T_2 - T_3 - T_4$
	Ring deformation	$S_{19} = T_1 + T_2 - T_3 - T_4$
	CH_2 rock	$S_{20} = \beta_1 + \beta_2 + \beta_3 + \beta_4 - \eta_1 - \eta_2 - \eta_3 - \eta_4$
	CH_2 rock	$S_{21} = \alpha_1 + \alpha_2 + \alpha_3 + \alpha_4 - \nu_1 - \nu_2 - \nu_3 - \nu_4$
	C–C symmetric stretch	$S_{22} = R_1 + R_2$
	Ring-C out-of-plane bend	$S_{23} = \mu_1 + \mu_2 - \mu_3 - \mu_4$
	Ring-C in-plane bend	$S_{24} = \mu_1 + \mu_2 + \mu_3 + \mu_4$
	CCC bend	$S_{25} = 5\theta - \sigma_1 - \sigma_2 - \pi_1 - \pi_2 - \delta$
	Torsion	$S_{26} = \tau_1 + \tau_2$
B	CH_2 antisymmetric stretch	$S_{27} = r_5 - r_6 - r_7 + r_8$
	CH_2 antisymmetric stretch	$S_{28} = r_9 - r_{10} - r_{11} + r_{12}$
	CH stretch	$S_{29} = r_3 - r_4$
	CH_2 symmetric stretch	$S_{30} = r_5 - r_6 + r_7 - r_8$
	CH_2 symmetric stretch	$S_{31} = r_9 - r_{10} + r_{11} - r_{12}$
	$^*CH_2$ antisymmetric stretch	$S_{32} = r_1 - r_2$
	CH_2 deformation	$S_{33} = 4\varphi_1 - 4\varphi_2 - \alpha_1 + \alpha_2 - \alpha_3 + \alpha_4 - \nu_1 + \nu_2 - \nu_3 + \nu_4$
	CH_2 deformation	$S_{34} = 4\varphi_3 - 4\varphi_4 - \beta_1 + \beta_2 - \beta_3 + \beta_4 - \eta_1 + \eta_2 - \eta_3 + \eta_4$
	CH in-plane bend	$S_{35} = 2\gamma_1 - 2\gamma_2 - \epsilon_1 + \epsilon_2 - \epsilon_3 + \epsilon_4$
	$^*CH_2$ wag	$S_{36} = \sigma_1 + \sigma_2 - \pi_1 - \pi_2$
	Ring breathing	$S_{37} = T_1 - T_2 + T_3 - T_4 + T_5 - T_6$
	CH_2 twist	$S_{38} = \alpha_1 - \alpha_2 - \alpha_3 + \alpha_4 - \nu_1 + \nu_2 + \nu_3 - \nu_4$
	CH_2 twist	$S_{39} = \beta_1 - \beta_2 - \beta_3 + \beta_4 - \eta_1 + \eta_2 + \eta_3 - \eta_4$
	CH out-of-plane bend	$S_{40} = \epsilon_1 - \epsilon_2 - \epsilon_3 + \epsilon_4$
	CH_2 wag	$S_{41} = \alpha_1 - \alpha_2 - \alpha_3 + \alpha_4 + \nu_1 - \nu_2 - \nu_3 + \nu_4$
	CH_2 wag	$S_{42} = \beta_1 - \beta_2 - \beta_3 + \beta_4 + \eta_1 - \eta_2 - \eta_3 + \eta_4$
	C–C antisymmetric stretch	$S_{43} = R_1 - R_2$
	Ring deformation	$S_{44} = T_1 - T_2 - T_3 + T_4$
	$^*CH_2$ rock	$S_{45} = \sigma_1 - \sigma_2 + \pi_1 - \pi_2$
	CH_2 rock	$S_{46} = \beta_1 - \beta_2 + \beta_3 - \beta_4 - \eta_1 + \eta_2 - \eta_3 + \eta_4$
	Ring deformation	$S_{47} = 2T_5 - 2T_6 - T_1 + T_2 - T_3 + T_4$
	CH_2 rock	$S_{48} = \alpha_1 - \alpha_2 + \alpha_3 - \alpha_4 - \nu_1 + \nu_2 - \nu_3 + \nu_4$
	Ring C in-plane bend	$S_{49} = \mu_1 - \mu_2 + \mu_3 - \mu_4$
	Ring out-of-plane bend	$S_{50} = \mu_1 - \mu_2 - \mu_3 + \mu_4$
	Torsion	$S_{51} = \tau_1 + \tau_2$

[a] Symmetry coordinates S_{32}, S_{45} and S_{51} belong to the A′ block whereas S_{11} and S_{26} to the A″ block for the C_s conformer.

Table 4
Observed and calculated frequencies for the *gauche–gauche* (C_2) and *gauche–gauche* (C_s) conformers of dicyclopropyl methane

Species	Fundamental		*Gauche–gauche* (C_2)							*Gauche–gauche* (C_s)						
			Ab initio[a]	Fixed scaled[b]	IR int.[c]	Raman act.[d]	dp ratio	Obs.[e]	PED[f]	Ab initio[a]	Fixed scaled[b]	IR int.[c]	Raman act.[d]	dp ratio	Obs.[e]	PED[f]
A	ν_1	CH_2 antisymmetric stretch	3298	3129	16.0	52.4	0.49	(3070)	$54S_1$, $45S_2$	3288	3119	0.8	128.8	0.74		$67S_1$, $33S_2$
	ν_2	CH_2 antisymmetric stretch	3286	3118	0.4	174.7	0.75	(3061)	$54S_2$, $45S_1$	3300	3131	22.8	50.7	0.50		$67S_2$, $33S_1$
	ν_3	CH stretch	3210	3045	4.0	225.9	0.05	(3006)	$84S_3$	3203	3039	31.8	49.7	0.63		$71S_3$, $26S_5$
	ν_4	CH_2 symmetric stretch	3203	3039	4.1	158.5	0.08	(2997)	$62S_4$, $24S_5$, $14S_3$	3200	3036	17.6	55.4	0.36		$82S_4$, $10S_3$
	ν_5	CH_2 symmetric stretch	3199	3035	11.5	22.9	0.72	(2990)	$69S_5$, $31S_4$	3209	3044	4.6	57.9	0.05		$67S_5$, $17S_3$, $15S_4$
	ν_6	$^*CH_2$ symmetric stretch	3067	2910	24.4	69.5	0.08	(2893)	$100S_6$	3068	2911	22.9	76.6	0.10		$99S_6$
	ν_7	CH_2 deformation	1574	1493	0.5	4.9	0.07	1461	$36S_7$, $39S_9$, $16S_{12}$	1526	1447	3.1	10.4	0.73	1428	$44S_7$, $48S_9$
	ν_8	$^*CH_2$ deformation	1545	1466	2.0	9.9	0.74	1441	$88S_8$	1545	1466	3.7	10.5	0.75	1441	$87S_8$
	ν_9	CH_2 deformation	1524	1446	3.0	9.2	0.74	1428	$48S_9$, $45S_7$	1577	1496	5.0	5.8	0.19	1464	$41S_9$, $35S_7$, $15S_{12}$
	ν_{10}	CH in-plane bend	1454	1380	0.9	6.9	0.13	1367	$43S_{10}$, $14S_{12}$, $12S_{11}$	1451	1377	0.3	10.7	0.32	1367	$51S_{10}$, $13S_{12}$
	ν_{11}	$^*CH_2$ twist	1321	1253	1.0	6.7	0.54	1257	$51S_{11}$, $10S_{15}$, $10S_{13}$	1308	1241	2.6	1.7	0.75	1250	$36S_{11}$, $18S_{36}$, $11S_{38}$
	ν_{12}	Ring breathing	1268	1203	0.0	38.9	0.13	1199	$50S_{12}$, $29S_{10}$	1280	1214	0.6	31.3	0.04	1204	$54S_{12}$, $24S_{10}$
	ν_{13}	CH_2 twist	1236	1173	0.5	15.4	0.74	1169	$19S_{13}$, $23S_{20}$, $24S_{21}$, $18S_{15}$, $13S_{14}$	1253	1188	0.1	4.3	0.69	1192	$17S_{13}$, $20S_{22}$, $14S_{24}$, $11S_{21}$, $12S_{45}$, $11S_{10}$
	ν_{14}	CH out-of-plane bend	1183	1122	0.1	2.4	0.21	1103	$55S_{14}$, $21S_{13}$	1180	1119	0.7	1.5	0.45	1103	$64S_{14}$, $17S_{13}$, $16S_{15}$
	ν_{15}	CH_2 twist	1158	1098	0.6	5.2	0.11	1093	$22S_{15}$, $17S_{11}$, $11S_{10}$, $11S_{22}$	1238	1174	1.7	11.6	0.74	1169	$24S_{15}$, $27S_{20}$, $18S_{21}$, $14S_{14}$, $13S_{13}$
	ν_{16}	CH_2 wag	1106	1050	2.0	0.9	0.74	1042	$50S_{16}$, $47S_{17}$	1106	1050	26.2	2.7	0.34	1042	$51S_{16}$, $34S_{17}$, $11S_{18}$
	ν_{17}	CH_2 wag	1099	1043	0.5	1.8	0.74	1020	$47S_{17}$, $42S_{16}$	1107	1050	2.7	1.1	0.52	1045	$60S_{17}$, $36S_{16}$
	ν_{18}	Ring deformation	998	947	0.8	15.0	0.58	935*	$50S_{18}$, $17S_{22}$	997	946	18.7	17.7	0.57	935*	$46S_{18}$, $18S_{19}$, $12S_{22}$
	ν_{19}	Ring deformation	990	940	1.4	19.8	0.66	928*	$40S_{19}$, $13S_{13}$, $17S_{20}$	884	839	11.5	7.4	0.65	831	$48S_{19}$, $12S_{20}$, $10S_{14}$
	ν_{20}	CH_2 rock	886	841	8.4	8.0	0.57	833	$22S_{20}$, $41S_{19}$, $12S_{18}$	918	872	0.0	7.9	0.62		$23S_{20}$, $31S_{45}$, $16S_{21}$
	ν_{21}	CH_2 rock	841	798	0.4	7.5	0.51	793	$53S_{21}$, $13S_{13}$, $10S_{18}$	818	777	3.7	1.3	0.05	780	$35S_{21}$, $19S_{45}$, $15S_{13}$, $10S_{18}$

Table 4 (*continued*)

Species	Fundamental		*Gauche–gauche* (C_2)							*Gauche–gauche* (C_s)						
			Ab initio[a]	Fixed scaled[b]	IR int.[c]	Raman act.[d]	dp ratio	Obs.[e]	PED[f]	Ab initio[a]	Fixed scaled[b]	IR int.[c]	Raman act.[d]	dp ratio	Obs.[e]	PED[f]
	ν_{22}	C–C symmetric stretch	796	755	0.0	9.5	0.53	754	$10S_{22}$, $31S_{15}$, $24S_{20}$, $11S_{18}$, $13S_{13}$	794	753	1.0	8.1	0.53	754	$11S_{22}$, $25S_{20}$, $31S_{15}$, $12S_{13}$, $11S_{18}$
	ν_{23}	Ring-C out-of-plane bend	462	439	0.5	5.3	0.52	452	$36S_{23}$, $27S_{25}$, $13S_{22}$	468	445	1.4	3.9	0.56	452	$37S_{23}$, $19S_{25}$
	ν_{24}	Ring-C in-plane bend	291	276	0.1	2.0	0.12	300*	$80S_{24}$, $10S_{22}$	353	337	0.2	3.1	0.14	345*	$54S_{24}$, $14S_{22}$, $10S_{25}$, $10S_{51}$
	ν_{25}	CCC bend	162	154	0.0	0.1	0.60	172*	$45S_{25}$, $47S_{23}$	164	156	0.1	0.0	0.71	172*	$43S_{25}$, $35S_{23}$, $15S_{24}$
	ν_{26}	Torsion	79	79	0.0	0.1	0.68	(108)	$92S_{26}$	67	67	0.0	0.0	0.75		$99S_{26}$
B	ν_{27}	CH_2 antisymmetric stretch	3298	3129	19.0	39.5	0.75	(3070)	$54S_{27}$, $45S_{28}$	3287	3118	0.1	49.8	0.75		$55S_{27}$, $45S_{28}$
	ν_{28}	CH_2 antisymmetric stretch	3286	3117	0.1	1.2	0.75	(3061)	$54S_{28}$, $45S_{27}$	3299	3129	13.9	31.0	0.75		$55S_{28}$, $45S_{27}$
	ν_{29}	CH stretch	3210	3045	10.4	45.5	0.75	(3006)	$87S_{29}$	3199	3035	2.3	5.9	0.75		$81S_{29}$, $18S_{30}$
	ν_{30}	CH_2 symmetric stretch	3203	3039	20.2	5.2	0.75	2997)	$56S_{30}$, $32S_{31}$, $11S_{29}$	3200	3036	8.3	16.2	0.75		$52S_{30}$, $40S_{31}$
	ν_{31}	CH_2 symmetric stretch	3199	3035	13.8	26.7	0.75	(2990)	$64S_{31}$, $36S_{30}$	3206	3042	3.7	22.3	0.75		$59S_{31}$, $29S_{30}$, $11S_{29}$
	ν_{32}	$^{*}CH_2$ antisymmetric stretch	3116	2956	23.0	63.9	0.75	(2913)	$99S_{32}$	3118	2958	23.3	68.4	0.73		$98S_{32}$
	ν_{33}	CH_2 deformation	1572	1491	2.0	2.9	0.75	1460	$39S_{33}$, $38S_{34}$, $16S_{37}$	1570	1490	0.4	1.8	0.75	1460	$40S_{33}$, $37S_{34}$, $17S_{37}$
	ν_{34}	CH_2 deformation	1526	1448	1.5	9.0	0.75	1428	$50S_{34}$, $50S_{33}$	1526	1447	3.1	7.2	0.75	1428	$50S_{34}$, $50S_{33}$
	ν_{35}	CH in-plane bend	1475	1399	1.3	5.1	0.75	1390	$34S_{35}$, $20S_{44}$, $14S_{36}$, $10S_{37}$	1480	1404	0.0	0.8	0.75	1390	$32S_{35}$, $19S_{43}$, $12S_{36}$, $10S_{34}$, $10S_{37}$
	ν_{36}	$^{*}CH_2$ wag	1348	1279	13.2	2.3	0.75	1285	$73S_{36}$, $14S_{35}$	1365	1295	6.1	2.8	0.75	1295	$58S_{36}$, $25S_{11}$
	ν_{37}	Ring breathing	1275	1209	0.9	10.1	0.75	1204	$52S_{37}$, $25S_{35}$	1266	1201	0.3	15.9	0.75	1195	$48S_{37}$, $28S_{35}$
	ν_{38}	CH_2 twist	1239	1175	0.7	0.8	0.75	1174	$29S_{38}$, $28S_{46}$, $10S_{43}$	1233	1170	0.2	4.8	0.75	1167	$19S_{38}$, $24S_{46}$, $24S_{48}$, $18S_{39}$, $15S_{40}$
	ν_{39}	CH_2 twist	1233	1170	0.4	0.5	0.75	1167	$29S_{39}$, $24S_{48}$, $12S_{43}$	1026	973	18.3	3.7	0.75	970	$10S_{39}$, $20S_{47}$, $18S_{43}$, $11S_{38}$, $10S_{48}$
	ν_{40}	CH out-of-plane	1178	1117	0.9	0.5	0.75	1103	$62S_{40}$, $18S_{38}$, $18S_{39}$	1175	1115	0.6	1.2	0.75	1103	$58S_{40}$, $21S_{39}$, $15S_{38}$
	ν_{41}	CH_2 wag	1106	1050	3.8	0.8	0.75	1045	$72S_{41}$, $23S_{42}$	1103	1047	0.5	0.3	0.75	1039	$61S_{41}$, $35S_{42}$
	ν_{42}	CH_2 wag	1101	1045	12.0	1.7	0.75	1015	$66S_{42}$, $16S_{41}$, $11S_{47}$	1086	1030	9.0	0.1	0.75	1010	$55S_{42}$, $28S_{41}$

Table 4 (*continued*)

Species	Fundamental		*Gauche–gauche* (C_2)							*Gauche–gauche* (C_s)						
			Ab initio[a]	Fixed scaled[b]	IR int.[c]	Raman act.[d]	dp ratio	Obs.[e]	PED[f]	Ab initio[a]	Fixed scaled[b]	IR int.[c]	Raman act.[d]	dp ratio	Obs.[e]	PED[f]
	ν_{43}	C–C antisymmetric stretch	1055	1000	28.4	2.7	0.75	994	$27S_{43}$, $20S_{47}$, $13S_{37}$	1129	1071	0.1	2.3	0.75	1064	$22S_{43}$, $16S_{35}$, $13S_{11}$, $11S_{37}$, $11S_{47}$
	ν_{44}	Ring deformation	977	927	3.6	17.8	0.75	923	$39S_{44}$, $17S_{48}$, $14S_{45}$, $11S_{38}$	946	898	4.6	9.2	0.75	879	$81S_{44}$
	ν_{45}	$^{*}CH_2$ rock	917	870	6.3	1.8	0.75	865	$18S_{45}$, $37S_{44}$, $12S_{40}$, $11S_{47}$	1070	1015	1.6	14.6	0.46	1002*	$17S_{45}$, $22S_{19}$, $14S_{23}$
	ν_{46}	CH_2 rock	859	815	7.2	6.3	0.75	815	$29S_{46}$, $20S_{40}$, $13S_{44}$, $10S_{38}$, $10S_{39}$	856	812	6.4	1.4	0.75	808	$29S_{46}$, $20S_{40}$, $13S_{44}$, $10S_{38}$
	ν_{47}	Ring deformation	834	792	14.3	3.7	0.75	784	$51S_{47}$, $17S_{45}$, $14S_{48}$	862	818	3.0	20.6	0.75	815	$55S_{47}$, $15S_{43}$, $15S_{48}$
	ν_{48}	CH_2 rock	809	767	0.3	1.8	0.75	773	$29S_{48}$, $24S_{39}$, $19S_{46}$, $18S_{38}$	809	768	0.3	3.1	0.75	773	$27S_{48}$, $23S_{46}$, $22S_{39}$, $18S_{38}$
	ν_{49}	Ring C in-plane bend	416	397	0.2	0.4	0.75	(409)	$74S_{49}$, $13S_{51}$	384	364	0.5	0.2	0.75		$78S_{49}$, $13S_{50}$
	ν_{50}	Ring C out-of-plane bend	348	330	0.8	0.4	0.75	345*	$85S_{50}$	309	293	0.3	0.4	0.75		$78S_{50}$, $13S_{49}$
	ν_{51}	Torsion	94	93	0.1	0.1	0.75	(140)	$82S_{51}$	101	98	0.0	0.1	0.03		$77S_{51}$

[a] Calculated with the MP2/G-31G(d) basis set.
[b] Scaled ab initio calculations with factor 0.9 for stretches and 0.9 for bends, and 1.0 for torsions using the MP2/6-31G(d) basis set.
[c] Calculated infrared intensities in km/mol.
[d] Calculated Raman activities in $Å^4$/amu.
[e] Values from the infrared spectrum of the xenon solution, except those in parentheses which are from the spectrum of the solid and those indicated with an asterisk, which are from the Raman spectrum of the liquid.
[f] For a description of the symmetry coordinates see Table 3.

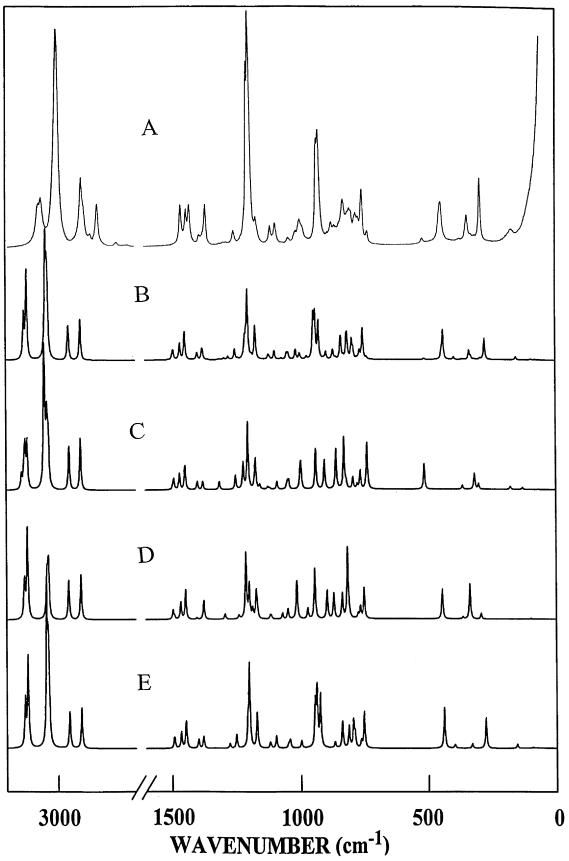

Fig. 5. Comparison of experimental and calculated Raman spectra of dicyclopropyl methane: (A) observed Raman spectra in the liquid phase; (B) calculated Raman spectrum of the mixture of conformers; (C) calculated Raman spectrum of the pure *cis–gauche* conformer; (D) calculated spectrum of the pure *gauche–gauche* (C_s) conformer; and (E) calculated infrared spectrum of the pure *gauche–gauche* (C_2) conformer.

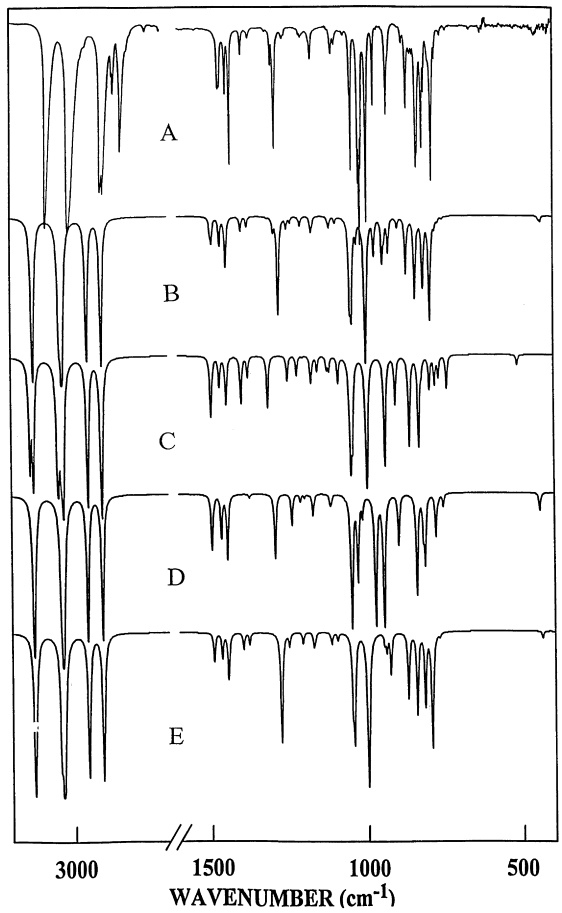

Fig. 6. Comparison of experimental and calculated infrared spectra of dicyclopropyl methane: (A) observed spectrum in liquid xenon at −80°C; (B) calculated spectrum of the mixture of conformers; (C) calculated spectrum of the pure *cis–gauche* conformer; (D) calculated spectrum of the pure *gauche–gauche* (C_s) conformer; and (E) calculated spectrum of the pure *gauche–gauche* (C_2) conformer.

present in the crystalline phase of dicyclopropyl methane.

In order to determine the enthalpy differences, ΔH, between the three stable conformers, a variable temperature study was undertaken using the infrared spectra of the sample dissolved in liquified noble gases. The spectra were recorded at 17 different temperatures in the ranges from −55 to −100°C for xenon and from −105 to −150°C for krypton solutions. The relative intensities of the bands at 994 and 865 cm^{-1}, assigned to the C_2 conformer, and those at 1295, 970 and 879 cm^{-1}, assigned to the C_s conformer, were measured as a function of temperature. The natural logarithms of the intensity ratios, $I(C_s)/I(C_2)$, were plotted versus the reciprocal of the absolute temperature, and the ΔH values were calculated from the slopes of the plots according to the van't Hoff equation; $-\ln K = (\Delta H/RT) - (\Delta S/R)$. In this equation K is substituted with the appropriate intensity ratio and ΔH is assumed to be independent of temperature. The data are summarized in Table 6, where ΔH values are listed

Table 5
Observed and calculated frequencies (cm^{-1}) for the *cis–gauche* (C_1) conformer of dicyclopropyl methane

Vib. no.	Description	Ab Initio[a]	Fixed scaled[b]	IR int.[c]	Raman act.[d]	dp ratio	Obs.[e]	PED[f]
ν_1	CH_2 antisymmetric stretch	3295	3126	2.7	73.5	0.73		$56S_1$, $28S_{27}$, $10S_{28}$
ν_2	CH_2 antisymmetric stretch	3310	3140	13.3	27.8	0.72		$45S_2$, $38S_{28}$
ν_3	CH stretch	3217	3052	12.6	211.3	0.04		$41S_3$, $21S_{29}$, $17S_4$, $10S_5$
ν_4	CH_2 symmetric stretch	3204	3039	6.0	66.0	0.13		$52S_4$, $17S_{31}$, $13S_{30}$
ν_5	CH_2 symmetric stretch	3199	3035	12.3	48.7	0.66		$34S_5$, $34S_{31}$, $17S_{30}$, $15S_4$
ν_6	$^*CH_2$ symmetric stretch	3068	2911	32.3	88.7	0.11		$100S_6$
ν_7	CH_2 deformation	1571	1491	0.8	6.7	0.23		$35S_7$, $33S_9$, $15S_{12}$
ν_8	$^*CH_2$ deformation	1548	1469	2.5	9.9	0.73		$92S_8$
ν_9	CH_2 deformation	1526	1448	3.4	9.4	0.72		$48S_9$, $45S_7$
ν_{10}	CH in-plane bending	1476	1400	4.2	4.6	0.44		$36S_{10}$, $17S_{36}$
ν_{11}	$^*CH_2$ twist	1320	1252	2.1	6.9	0.53		$59S_{11}$
ν_{12}	Ring breathing	1269	1204	0.1	31.7	0.12		$49S_{12}$, $20S_{10}$
ν_{13}	CH_2 twist	1149	1090	2.2	3.3	0.74		$23S_{13}$, $13S_{20}$, $12S_{10}$, $11S_{45}$
ν_{14}	CH out-of-plane bend	1186	1126	1.0	1.2	0.45		$54S_{14}$, $20S_{15}$, $11S_{13}$
ν_{15}	CH_2 twist	1241	1177	1.9	3.9	0.68		$19S_{15}$, $23S_{20}$, $22S_{21}$, $19S_{13}$, $15S_{14}$
ν_{16}	CH_2 wag	1107	1050	9.7	0.9	0.65		$60S_{16}$, $14S_{41}$, $10S_{42}$
ν_{17}	CH_2 wag	1110	1053	1.0	0.6	0.65		$56S_{17}$, $22S_{16}$, $11S_{41}$
ν_{18}	Ring deformation	991	940	13.2	14.1	0.60	958	$37S_{18}$, $13S_{22}$
ν_{19}	Ring deformation	907	861	9.7	12.5	0.74		$43S_{19}$, $24S_{44}$, $10S_{45}$
ν_{20}	CH_2 rock	838	795	2.8	3.3	0.58		$40S_{20}$, $11S_{47}$, $11S_{15}$
ν_{21}	CH_2 rock	820	778	2.3	1.2	0.19		$38S_{21}$, $19S_{13}$, $15S_{45}$
ν_{22}	C–C symmetric stretch	779	739	2.8	12.0	0.37	738	$27S_{22}$, $27S_{18}$, $11S_{15}$
ν_{23}	Ring-C out-of-plane bend	382	364	0.3	0.4	0.06		$29S_{23}$, $28S_{49}$, $14S_{24}$
ν_{24}	Ring-C in-plane bend	334	317	0.4	1.3	0.27		$38S_{24}$, $34S_{23}$, $11S_{50}$
ν_{25}	CCC bend	186	177	0.1	0.1	0.22		$49S_{25}$, $21S_{49}$, $13S_{50}$
ν_{26}	Torsion	67	67	0.0	0.1	0.72		$92S_{26}$
ν_{27}	CH_2 antisymmetric stretch	3299	3130	17.3	41.0	0.63		$41S_{27}$, $23S_2$, $18S_{28}$, $17S_1$
ν_{28}	CH_2 antisymmetric stretch	3287	3118	0.2	89.0	0.75		$32S_{28}$, $26S_2$, $23S_{27}$, $18S_1$
ν_{29}	CH stretch	3198	3034	18.4	27.9	0.75		$46S_{29}$, $48S_3$
ν_{30}	CH_2 symmetric stretch	3207	3042	8.6	86.6	0.15		$60S_{30}$, $16S_5$, $14S_4$
ν_{31}	CH_2 symmetric stretch	3214	3049	11.2	97.8	0.26		$43S_{31}$, $301S_5$, $18S_{29}$
ν_{32}	$^*CH_2$ antisymmetric stretch	3115	2955	25.1	76.6	0.74		$99S_{32}$
ν_{33}	CH_2 deformation	1577	1496	5.5	1.7	0.70		$38S_{33}$, $31S_{34}$, $15S_{32}$
ν_{34}	CH_2 deformation	1524	1446	1.3	6.8	0.74		$50S_{34}$, $44S_{33}$
ν_{35}	CH in-plane bend	1454	1379	1.7	4.6	0.54		$39S_{35}$, $12S_{43}$, $11S_{32}$
ν_{36}	$^*CH_2$ wag	1386	1315	4.7	4.3	0.51	1312	$54S_{36}$
ν_{37}	Ring breathing	1288	1222	1.6	12.7	0.50		$40S_{37}$, $30S_{35}$
ν_{38}	CH_2 twist	1237	1174	0.7	12.3	0.75		$19S_{38}$, $26S_{46}$, $22S_{48}$, $18S_{40}$, $14S_{39}$
ν_{39}	CH_2 twist	1220	1157	1.2	1.9	0.68		$18S_{39}$, $11S_{43}$
ν_{40}	CH out-of-plane bend	1179	1119	1.1	0.6	0.75		$47S_{40}$, $24S_{38}$, $13S_{39}$
ν_{41}	CH_2 wag	1106	1049	3.8	2.0	0.31		$34S_{41}$, $31S_{17}$, $23S_{42}$
ν_{42}	CH_2 wag	1101	1044	8.1	3.4	0.60		$46S_{42}$, $30S_{41}$, $12S_{47}$
ν_{43}	C–C antisymmetric stretch	1053	999	15.8	6.5	0.72		$17S_{43}$, $16S_{47}$
ν_{44}	Ring deformation	954	906	4.3	9.7	0.74		$54S_{44}$, $11S_{46}$
ν_{45}	$^*CH_2$ rock	1050	996	5.7	7.0	0.24		$10S_{45}$, $10S_{22}$, $10S_{18}$,
ν_{46}	CH_2 rock	807	766	1.7	4.9	0.75		$19S_{46}$, $21S_{48}$, $20S_{39}$, $19S_{38}$
ν_{47}	Ring deformation	874	830	9.7	15.4	0.72		$16S_{47}$, $19S_{19}$
ν_{48}	CH_2 rock	865	821	0.9	1.7	0.70		$26S_{48}$, $16S_{40}$, $13S_{47}$
ν_{49}	Ring C in-plane bend	541	514	0.8	4.1	0.60	521	$13S_{49}$, $25S_{25}$, $15S_{24}$, $11S_{22}$
ν_{50}	Ring C out-of-plane bend	317	301	0.6	0.4	0.34		$56S_{50}$, $16S_{49}$, $15S_{24}$
ν_{51}	Torsion	131	129	0.0	0.1	0.13		$76S_{51}$

[a] Calculated with the MP2/G-31G(d) basis set.
[b] Scaled ab initio calculations with factor 0.9 for stretches and 0.9 for bends, and 1.0 for torsions using the MP2/6-31G(d) basis set.
[c] Calculated infrared intensities in km/mol.
[d] Calculated Raman activities in $Å^4$/amu.
[e] Values from the infrared spectrum of the xenon solution, except those in parentheses which are from the spectrum of the solid and those indicated with an asterisk, which are from the Raman spectrum of the liquid.
[f] For a description of the symmetry coordinates see Table 3.

Table 6
Temperature and intensity ratios for the conformational study of dicyclopropyl methane in the C_2 and C_s conformations

T (°C)	1000/T/K	$-I$(970/994)	$-I$(879/865)	$-I$(879/994)	$-I$(970/865)	$-I$(1295/865)	$-I$(1295/994)
−55	4.59	1.6363	1.9410	3.5656	0.0117	1.7841	2.4885
−60	4.69	1.5078	1.9150	3.5344	−0.1116	1.8134	2.5385
−65	4.81	1.5323	1.9198	3.5430	−0.0908	1.8234	2.5789
−70	4.93	1.6928	2.0261	3.6445	0.0745	1.8292	2.6191
−75	5.05	1.7083	2.0552	3.6677	0.0927	1.8289	2.6525
−80	5.18	1.7411	2.1121	3.7339	0.1193	1.8677	2.7196
−85	5.32	1.7606	2.1081	3.7355	0.1331	1.9032	2.7914
−90	5.46	1.7957	2.2022	3.8407	0.1571	1.9585	2.8685
−95	5.62	1.7921	2.3222	3.9456	0.1686	1.9566	2.8854
ΔH (cm^{-1})[a]		179 ± 41	261 ± 27	266 ± 28	173 ± 41	274 ± 7	280 ± 11
−110	6.13	2.1006	2.1415	3.9462	0.2959	1.2850	3.0901
−115	6.33	1.9745	2.2627	4.0582	0.1790	3.3565	3.1520
−120	6.54	2.0249	2.3354	4.1344	0.2259	1.40147	3.2003
−125	6.76	2.0395	2.4035	4.1928	0.2501	1.5211	3.3104
−130	6.99	2.1690	2.4463	4.2311	0.3842	1.6054	3.3902
−135	7.25	2.1313	2.5739	4.358	0.3465	1.6967	3.4814
−140	7.52	2.3342	2.7160	4.5011	0.5490	1.7978	3.5830
−145	7.81	2.3918	2.6240	4.4153	0.6006	1.9050	3.6963
ΔH (cm^{-1})[b]		153 ± 35	219 ± 27	216 ± 26	159 ± 34	261 ± 6	254 ± 5

[a] Average value of ΔH is 239 ± 13 cm^{-1} (2.86 ± 0.16 kJ/mol) with the C_2 the more stable form in xenon.
[b] Average value of ΔH is 211 ± 12 cm^{-1} (2.52 ± 0.14 kJ/mol) with the C_2 the more stable form in krypton.

for each combination of conformer bands in xenon and krypton solutions. The values are consistent with each other and result in average values of 239 ± 13 and 211 ± 12 cm^{-1} for the enthalpy differences between the C_2 and C_s conformers in xenon and krypton, respectively, with the C_2 form being more stable.

The low signal-to-noise ratios of the observed bands for the C_1 conformer resulted in poor least-squares fits of the intensity data. Therefore, an alternative method of determining the ΔH was applied by using the calculated (MP2/6-31G(d)) and observed infrared intensities of the above mentioned bands of the C_2 and C_s conformers and the bands at 1312, 958 and 736 cm^{-1} assigned to the C_1 conformer. By direct substitution of these data in the van't Hoff equation for each of the utilized temperatures, ΔH values of 479 ± 84 and 275 ± 112 cm^{-1} were obtained between the C_1 and C_2 and the C_1 and C_s forms, respectively, with the C_1 form being the least stable. This procedure yields ΔH of 204 cm^{-1} for the C_s/C_2 conformer pair which is consistent with the results from the van't Hoff plots within the experimental error.

5. Vibrational assignment

The four conformers of dicyclopropyl methane have different point groups of symmetry which makes it easier to assign their vibrational spectra. Since the *cis–cis* (C_{2v}) conformer was not observed due to its very high energy, it will not be considered in this discussion. One of the *gauche–gauche* forms has C_2 symmetry with 26 A and 25 B normal modes. The fundamentals from the A block should produce polarized Raman bands and B-type infrared band contours, whereas the fundamentals from the B block should be depolarized in the Raman spectra and give rise to A/C-type hybrid band envelopes. The other *gauche–gauche* (C_s) conformer has C_s point group symmetry. Its 27 A′ vibrations should be polarized and yield B/C-type band contours whereas the 24 A″ modes should be depolarized and produce A-type infrared band contours. Since the *cis–gauche* (C_1) conformer has the trivial C_1 symmetry its vibrations cannot be classified as those of the C_2 and C_s forms, but all Raman lines should be polarized and the infrared band contours will be hybrid A/B/C-types.

The vibrational assignment of dicyclopropyl methane has been proposed previously by Kalasinsky et al. [7]. Therefore, we will discuss here only the major discrepancies between this earlier assignment and those proposed herein. The complete assignments are given in Table 1. In addition, we will point out bands observed in the noble gas solutions that have not been observed previously, as well as new bands from the spectra of the solid phase which was more completely annealed in this study compared to the previous one [7].

The methylene CH_2 deformation has been assigned [7] as the highest frequency deformation mode at 1462 cm^{-1}, whereas our normal coordinate analysis shows that it falls at a lower (1443 cm^{-1}) frequency with the 1462 band assigned instead to a ring CH_2 deformation. The band at 1295 cm^{-1} in the spectra of the xenon solution, which was previously reported but not assigned in the infrared spectrum of the liquid, is now assigned to the methane CH_2 wag of the C_s conformer. In addition, a much weaker band at 1312 cm^{-1} is attributed to the same mode of the C_1 form. The latter two bands vanish in the spectra of the solids. Another fundamental of the C_s conformer was observed at 1250 cm^{-1} (methylenic CH_2 twist) in the spectra of the xenon solution with a corresponding Q-branch at 1253 cm^{-1} in the infrared spectrum of the gas. Since the methylene CH_2 twist (ν_{11}) of the C_2 conformer is from the A block, its band contour should be B-type, so the Q-branch can only be due to the fundamental of the C_s form.

The authors of the previous vibrational study [7] suggested that the strong Raman band at 1206 cm^{-1} is due to the ring breathing vibrations of the less stable (second) conformer with the lower frequency band at 1199 cm^{-1} assigned to the same mode of the more stable form. Our analysis shows that the two bands are actually due to overlapping ring breathing modes of both conformers (Table 1). The totally symmetric modes, ν_{12} and ν'_{12}, where the prime indicates a mode of the C_s conformer, are expected to be strongly polarized and 2–4 times stronger than the antisymmetric vibrations, ν_{37} and ν'_{37} which are depolarized (Table 4). However, the contribution of the antisymmetric modes to the two Raman bands may still be significant and makes them questionable candidates for variable temperature studies.

One of the four ring CH_2 twisting fundamentals, ν_{15}, which has been previously [7] assigned at 1169 cm^{-1}, is now shifted to a lower wavenumber at 1093 cm^{-1} in the spectrum of the xenon solution. The corresponding Raman band at 1094 cm^{-1} is completely polarized as expected for this fundamental.

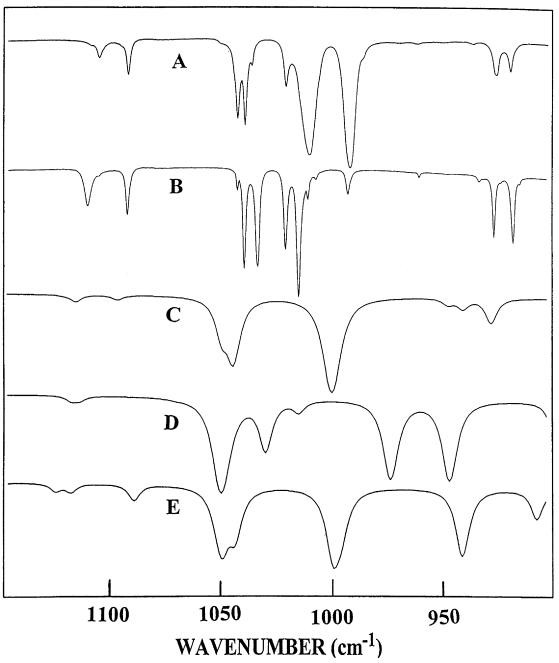

Fig. 7. Infrared spectra of dicyclopropyl methane: (A) after three cycles of annealing; (B) second annealed material which was obtained from liquid; (C) predicted spectrum of the C_2 conformer; (D) predicted spectrum of the C_s conformer; and (E) predicted spectrum of the C_1 conformer.

There are eight expected fundamentals of the C_2 and C_s conformers (all ring CH_2 wags) in the region between 1050 and 1000 cm^{-1}. Seven of them are predicted by the ab initio calculations to be almost coincident at ~1045 cm^{-1} and one (belonging to the C_s form) is predicted at ~1030 cm^{-1}. The observed infrared spectrum of the gas in this region consists of two clusters of bands, one weaker band at ~1045 cm^{-1} and a much stronger and more complex band contour centered at ~1020 cm^{-1}. The intensity of the latter band is quite surprising in light of the calculated infrared intensities listed in Table 4, which causes a significant discrepancy between the observed and calculated infrared spectra (Fig. 7) in this region. Nevertheless, in the infrared spectrum of the annealed solid there are four distinct bands at

1040, 1034, 1021 and 1015 cm^{-1} that must be tentatively assigned to the four CH_2 wags of the C_2 conformer. The band at 1010 cm^{-1} observed in the infrared spectrum of the xenon solution seems to gradually disappear upon annealing in the spectra of the solid (Fig. 7). This band is assigned to the A″ CH_2 wag of the C_s form predicted at 1030 cm^{-1}. The nearby Raman band at 1002 cm^{-1}, which appears to be polarized in the Raman spectrum of the liquid is not present in the spectra of the solid and is assigned to methylene CH_2 wag of the same conformer.

In the infrared spectrum of the gas there are two A-type bands with Q-branches at 884 and 868 cm^{-1}. One of them can be assigned to the CH_2 rock of the C_2 conformer, but the second band must be assigned to the C_s form since the C_2 conformer has no other vibration from the B symmetry block that can produce a Q-branch in the 850–900 cm^{-1} region. On the other hand, the higher frequency band vanishes from the spectrum of the annealed solid, and therefore it is assigned to the C_s form. The authors of the previous vibrational study [7] have assigned this band to a fundamental of the C_2 conformer, assuming that it shifts to ~865 cm^{-1} in the solid phase where the second band shifts to 856 cm^{-1}. It is more reasonable to assume that the band at 868 cm^{-1} in the gas phase (865 cm^{-1} in xenon solution) corresponds to the band at 865 cm^{-1} in the spectrum of the solid phase. The band at 856 cm^{-1} in the spectrum of the solid can then be attributed to either solid phase splitting or a combination band in Fermi resonance with ν_{45}, with the latter more probable.

According to our normal coordinate analysis we have described the fundamentals at 784 and 773 cm^{-1} as a ring deformation and ring CH_2 rock, respectively, rather than ring CH_2 rock and methylene CH_2 rock as suggested in the previous study [7]. In addition, the CCC bend is assigned to the band at 172 cm^{-1} in the Raman spectrum of the liquid, which is a fundamental from the A symmetry block of the C_2 conformer. The previous assignment [7] for this band was to a fundamental of the B block due to the high value of the observed depolarization-ratio. However, our calculations (Table 4) show that the CCC bending fundamentals, whether from the A (or A′) block, have quite high depolarization ratios of 0.60 and 0.71 for the C_2 and C_s forms, respectively, and they are the only fundamentals expected in the 150–200 cm^{-1} range.

6. Discussion

In the initial vibrational study [7] of dicyclopropyl methane, it was concluded that only the C_2 and C_s conformers with the *gauche* orientation existed in the fluid phases with the C_2 conformer the more stable form. However, utilizing the predicted frequencies from the ab initio calculations along with the vibrational data from the rare gas solutions it is clear that a third conformer is present in a relatively small concentration (7%) in the fluid phases. The relatively large uncertainty of ±84 cm^{-1} associated with the ΔH value obtained from the two fundamentals of the C_1 form with three fundamentals from the C_2 form is the result of the low intensity of the two vibrations of the C_1 conformer. Nevertheless, from the relative intensities of the fundamentals for the C_1 conformer compared to those for the two more stable conformers one obtains the predicted infrared intensities from the ab initio MP2/6-31(d) calculations. In addition, the ΔH values obtained from the studies in xenon and krypton are in excellent agreement with the ab initio energy calculations.

The infrared and Raman bands in the spectra of the crystalline material reported in the earlier spectroscopic study [7] were not nearly as sharp as those found in the current vibrational study. However, it was possible to reproduce the previously reported [7] spectra. These spectra were obtained by direct deposition of the gaseous sample on the solid substrates of either the infrared or Raman cells, producing an amorphous material. Subsequent annealing was carried out by bringing the sample near the melting point and then cooling it to near the temperature of boiling liquid nitrogen. After performing this cycling process approximately three times, a solid sample was obtained which gave a spectrum that was the same as that previously reported [7] for the solid. However, it was clear that the solid was not a crystalline material since the low frequency Raman spectrum had no lattice modes (Fig. 8). It is possible that this solid is a polymorph with disorder since visually it appeared to be a crystalline solid. However, by permitting the sample to melt and then rapidly

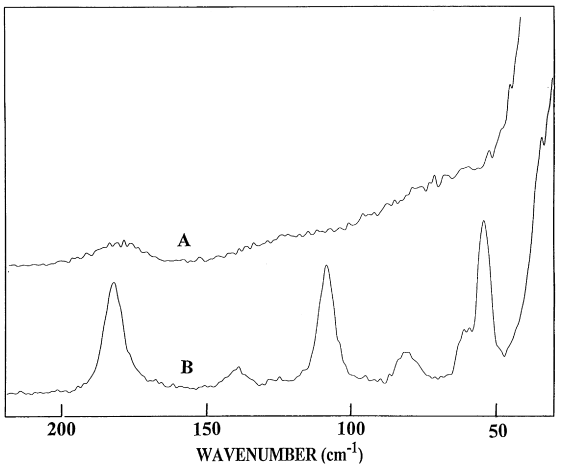

Fig. 8. Low frequency Raman spectra of dicyclopropyl methane: (A) amorphous solid; and (B) annealed solid.

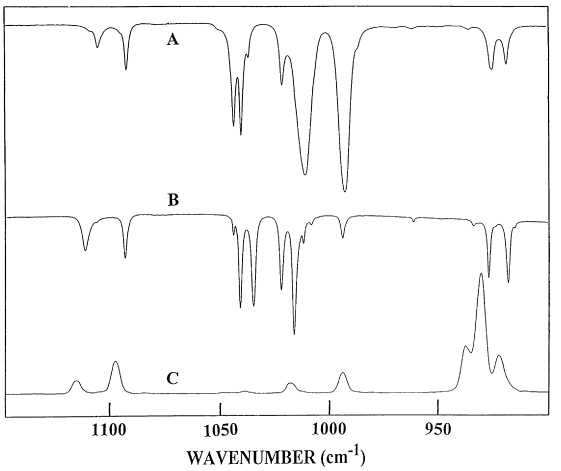

Fig. 9. Spectra of dicyclopropyl methane: (A) infrared spectrum of first annealed solid; (B) infrared spectrum of second annealed solid; and (C) Raman spectrum of annealed solid.

freezing it, the crystalline solid was obtained which has a significantly different spectrum in the 1000 cm^{-1} region and several clearly discernible lattice modes in the low frequency Raman spectrum of the solid (Fig. 8).

Several bands that are present in the spectrum of the first solid disappear, shift, or become very weak in the spectrum of the second polycrystalline solid. For example, in the carbon–hydrogen stretching region bands at 3076, 3056, 2903 and 2843 cm^{-1} are not present in the spectrum of the second solid. Similarly, in the carbon–hydrogen deformation region bands at 1454, 1434 and 1429 cm^{-1}, which are pronounced absorption bands in the spectrum of the first solid, are absent or shifted in the spectrum of the polycrystalline solid. Therefore, the significant spectral changes observed in the 900–1100 cm^{-1} region are also found throughout the entire spectrum but are not as pronounced as those shown in Fig. 7. We attempted to assign the spectrum of the second solid to that of the C_s or C_1 conformers but the data were most consistent with that predicted for the C_2 form (Fig. 7).

The Raman and infrared spectral data are very complementary in most of the spectral regions. For example, in Fig. 9 both spectra are shown and many of the infrared bands which are quite pronounced are quite weak in the Raman spectrum, whereas many of the pronounced Raman lines have relatively weak infrared counterparts. These differences show up best in the spectra of the solid where the infrared and Raman bands are relatively sharp. In the spectra of the fluid phases the bands are quite broad and, with such a large number of fundamentals falling in relatively narrow ranges, it is not so evident that both the Raman and infrared spectral data are necessary to assign these closely spaced fundamentals.

The PED for the C_2 conformer indicates extensive mixing of the modes in the 700–1400 cm^{-1} region. For example, ν_{13} which has been assigned as a CH_2 twist has only 19% contribution from this motion with 23% CH_2 rock, 24% of the other ring CH_2 rock, 15% CH_2 twist and 13% CH bend. Similar distributions are also found for ν_{15}, ν_{20} and ν_{22} in the A symmetry block along with extensive mixing in ν_{38}, ν_{39}, ν_{43}, ν_{45}, ν_{46} and ν_{48} of the B symmetry block. For the C_s conformer the mixing is even more extensive. Therefore, the descriptions provided for these modes are more for "book-keeping" than for providing the actual atomic motions involved.

There is little difference in the force constants for the three identified conformers of dicyclopropyl methane. For this reason most of the fundamentals are predicted at nearly the same frequency for all three conformers. Where differences are predicted, such as in the low frequency region, it is usually

due to differences in the mixing of the vibrational motions rather than differences in the internal coordinate force constants among the conformers.

The structural parameters obtained from the ab initio MP2/6-311+G(d,p) calculations (Table 2) are expected to be close to the actual parameters, i.e. distances within ±0.005 Å and angles within 0.5°. This prediction is based on the similar parameter values obtained for propane and oxirane from the corresponding calculations which could be compared to the experimental values [18]. Therefore, it is expected that these parameters are as good as one could obtain from an electron diffraction or extensive microwave study of this molecule. Finally, it should be noted that, with the exception of the parameters associated with the orientation of the cyclopropyl rings, there is little difference in the structural parameters for the three identified conformers of dicyclopropyl methane.

The fact that one of the conformers (C_1) found in the fluid phases has the *cis* orientation of one of the three-membered rings indicates some possible interaction between the three-membered rings' orbitals. For example, in monosubstituted methylcyclopropane molecules it is found that the ethynyl and cyanide groups lead to large amounts of the *cis* conformer compared to the amounts of this conformer present in chloro- and bromomethyl cyclopropane. Although it has been suggested that the electronegativity of the substituent may be the controlling factor [6], it is probably an interaction of the substituent with the three-membered ring in some fashion that leads to significant amounts of a more stabilized *cis* conformer compared to the amount of *gauche* conformer present in these molecules. This possible interaction no doubt merits further investigation, both theoretically as well as experimentally.

Acknowledgements

J.R.D. acknowledges the University of Kansas City Trustees for a Faculty Fellowship award for partial financial support of this research.

References

[1] J.R. Durig, Z. Yu, X. Zhu, G.A. Guirgis, Submitted for publication.
[2] J.R. Durig, S. Shen, X. Zhu, C.J. Wurrey, J. Mol. Struct. 485 (1999) 501.
[3] C.J. Wurrey, S. Shen, T.K. Gounev, J.R. Durig, J. Mol. Struct. 406 (1997) 207.
[4] C.J. Wurrey, S. Shen, X. Zhu, H. Zhen, J.R. Durig, J. Mol. Struct. 449 (1998) 203.
[5] G.A. Guirgis, C.J. Wurrey, Z. Yu, X. Zhu, J.R. Durig, J. Phys. Chem. 103 (1999) 1509.
[6] W. Caminati, R. Danieli, M. Dakkouri, R. Bitschenauer, J. Phys. Chem. 99 (1995) 1867.
[7] V.F. Kalasinsky, J.L. Pool, N.S. Eymann, J.T. Leahey, M.D. Weakley, Y.Y. Yeh, C.J. Wurrey, Spectrochim. Acta 42A (1986) 149.
[8] C. Møller, M.S. Plesset, Phys. Rev. 46 (1934) 618.
[9] F.A. Miller, B.M. Harney, Appl. Spectrosc. 24 (1970) 291.
[10] M.J. Frisch, G.W. Trucks, H.B. Schlegel, G.E. Scuseria, M.A. Robb, J.R. Cheeseman, V.G. Zakrzewski, J.A. Montgomery Jr., R.E. Stratmann, J.C. Burant, S. Dapprich, J.M. Millam, A.D. Daniels, K.N. Kudin, M.C. Strain, O. Farkas, J. Tomasi, V. Barone, M. Cossi, R. Cammi, B. Mennucci, C. Pomelli, C. Adamo, S. Clifford, J. Ochterski, G.A. Petersson, P.Y. Ayala, Q. Cui, K. Morokuma, D.K. Malick, A.D. Rabuck, K. Raghavachari, J.B. Foresman, J. Cioslowski, J.V. Ortiz, B.B. Stefanov, G. Liu, A. Liashenko, P. Piskorz, I. Komaromi, R. Gomperts, R.L. Martin, D.J. Fox, T. Keith, M.A. Al-Laham, C.Y. Peng, A. Nanayakkara, M.W. Wong, J.L. Andres, C. Gonzalez, M. Challacombe, P.M.W. Gill, B. Johnson, W. Chen, M.W. Wong, J.L. Andres, M. Head-Gordon, E.S. Replogle, J.A. Pople, GAUSSIAN-98 (Revision A.6), Gaussian Inc., Pittsburgh, PA, 1998.
[11] P. Pulay, Mol. Phys. 17 (1969) 197.
[12] J.H. Schachtschneider, Vibrational Analysis of Polyatomic Molecules: Parts V and VI. Technical Report Nos. 231, 57, Shell Development Co., Houston, TX, 1964, 1965.
[13] G.A. Guirgis, X. Zhu, Z. Yu, J.R. Durig, J. Phys. Chem. 104 (2000) 4383.
[14] M.J. Frisch, Y. Yamaguchi, J.F. Gaw, H.F. Schaefer III, J.S. Binkley, J. Chem. Phys. 84 (1986) 531.
[15] R.D. Amos, Chem. Phys. Lett. 124 (1986) 376.
[16] G.W. Chantry, in: A. Anderson (Ed.), The Raman Effect, vol. 1, Marcel Dekker, New York, 1971 (chap. 2).
[17] P.L. Polavarapu, J. Phys. Chem. 94 (1990) 8106.
[18] J.R. Durig, in: M. Hargittai (Ed.), Advances in Molecular Structure Research, vol. 6, JAI Press, Stamford, CT, 2000, pp. 401–442.